Developmental and Comparative Immunology 103 (2020) 103528

Contents lists available at ScienceDirect

Developmental and Comparative Immunology

journal homepage: www.elsevier.com/locate/devcompimm

# Identification and characterization of IRF9 from black carp *Mylopharyngodon piceus*

Xingyu Lu[1], Ji Liu[1], Jun Yan, Hui Wu, Hao Feng*

*State Key Laboratory of Developmental Biology of Freshwater Fish, College of Life Science, Hunan Normal University, Changsha, 410081, China*

ARTICLE INFO

*Keywords:*
Black carp
IRF9
STAT1
Innate immunity

ABSTRACT

Interferon regulatory factor 9 (IRF9) plays a crucial role in JAK-STAT signaling in human and mammal. However, the relationship between IRF9 and STAT1 in teleost fish remains largely unknown. The previous study has elucidated that two STAT1 isoforms (bcSTAT1a and bcSTAT1b) of black carp (*Mylopharyngodon piceus*) play an important role during the innate immune activation initiated by grass carp reovirus (GCRV). In this paper, black carp IRF9 (bcIRF9) has been identified and characterized. bcIRF9 was distributed majorly in the nucleus and the linker domain (LD) of bcIRF9 was vital for its nuclear localization. bcIRF9 showed ISRE-inducing activity in reporter assay and presented antiviral activity against GCRV in plaque assay, in which both DNA binding domain (DBD) and LD of bcIRF9 were essential for its antiviral signaling. bcIRF9 was identified to interact with both bcSTAT1a and bcSTAT1b in the co-immunoprecipitation assay. It was interesting that bcIRF9-mediated antiviral signaling was up-regulated by bcSTAT1a; however, down-regulated by bcSTAT1b. Thus, our data support the conclusion that bcIRF9 plays an important role in the innate immune defense against GCRV, in which two STAT1 proteins function differently.

## 1. Introduction

Innate immunity is the first line of host defense against pathogen infection in vertebrates (Chiang and Liu, 2018). The host cells recruit the pathogen recognition receptors (PRRs) to recognize the invading pathogens and activate the downstream signaling pathway to trigger the expression of type I interferons (IFNs), which include Toll-like receptors (TLRs) and retinoic acid-inducible gene I (RIG-I)-like receptors (RLRs) (Xu et al., 2019). IFNs are a group of small, induce-expressed cytokines, which play key the roles in both innate and adaptive immune responses (Ivashkiv and Donlin, 2014). The secreted IFNs stimulate either the host cell itself through autocrine, or the neighbor cells through paracrine, to induce the production of IFN-stimulated genes (ISGs), which finally initiate the innate immune response (Pervolaraki et al., 2018).

In humans and mammals, Janus kinase (JAK)-signal transducer and activator of transcription (STAT) signaling pathway plays the key role in IFN-mediated ISGs expression, most of which are antiviral proteins and pro-inflammatory cytokines (Yuan et al., 2018). After the binding of IFNs, the *trans*-membrane interferon receptors (IFNRs) activate the associated intracellular tyrosine kinases (JAK1, TYK2) and phosphorylate signal transducer and activator of transcription 1 (STAT1) and STAT2, which interact with IRF9 and form STAT1/STAT2/IRF9 trimeric complex, named IFN-stimulated gene factor 3 (ISGF3) (Suprunenko and Hofer, 2016). ISGF3 translocate from cytoplasm to the nucleus and trigger the transcription of most ISGs by binding to the IFN-stimulated response element (ISRE), which is a conserved component of the promoter of many ISGs (Najjar and Fagard, 2010).

Interferon regulatory factors (IRFs) play a pivotal role in both innate and adaptive immunity, including the development of immune cells and induction of cytokines (Yanai et al., 2012). The vertebrate IRF family consists of eleven members, in which IRF11 is exclusively found in fish, and is classified into IRF1, IRF3, IRF4 and IRF5 subfamilies, with IRF1, IRF2 and IRF11 belonging to IRF1 subfamily, IRF3 and IRF7 belonging to IRF3 subfamily, IRF4, IRF8, IRF9 and IRF10 belonging to IRF4 subfamily, IRF5 and IRF6 belonging to IRF5 subfamily (Huang et al., 2010). All IRF members possess a highly conserved N-terminal DBD, which is composed of five conserved tryptophan repeats and forms a helix-loop-helix motif to recognize consensus tandem repeat of (5′-AANNGAAA-3′) (Yanai et al., 2012). Besides, most IRF members (except IRF1 and IRF2) have a C-terminal IAD, which is involved in the association with homologous or heterogenous proteins for the induction of IFN or ISGs (Paun and Pitha, 2007). Based on a comparison of the C-terminal region of the IRF proteins, IRF1, IRF3 and IRF9 have been

* Corresponding author.
*E-mail address:* fenghao@hunnu.edu.cn (H. Feng).
[1] These authors contribute equally to this paper.

https://doi.org/10.1016/j.dci.2019.103528
Received 6 September 2019; Received in revised form 21 October 2019; Accepted 21 October 2019
Available online 22 October 2019
0145-305X/ 

**Table 1**
Primers used in the study.

| Primer name | Sequence (5′-3′) | Primer information |
|---|---|---|
| bcIRF9-N-F | ACTGACGGTACCATGGCATCTGGAAGGATTCG | Gene cloning |
| bcIRF9-N-R | ACTGACCTCGAGTTAACAAAGATTCAGCGTCAC | |
| bcIRF9-ΔDBD-N-F | ACTGACGGTACCATGGGAGTGGTGAAAATAAAAAAAG | Gene cloning |
| bcIRF9-ΔLD-N-F | ACTGACGGTACCTAGAAGAACAAGTGCTGAACTCTTTCC | Gene cloning |
| bcIRF9-ΔLD-N-R | ACTGACCTCGAGGGAAAGAGTTCAGCACTTGTTCTTCTA | |
| bcIRF9-ΔIAD-N-R | ACTGACCTCGAGTTATCTCTTTTCTTCTGAC | Gene cloning |
| CMV-F | CGCAAATGGGCGGTAGGCGTG | |
| BGH-R | TAGAAGGCACAGTCGAGG | |
| bc-Q-actin-F | TGGGCACTGCTGCTTCCT | q-PCR |
| bc-Q-actin-R | TGTCCGTCAGGCAGCTCAT | |
| bcIRF9-Q-F | GAGGAAGATGCGGCTATT | q-PCR |
| bcIRF9-Q-R | TGGACTTTTGTTGAGGGC | |

described as activators, whilst IRF2, IRF4, IRF5, IRF7 and IRF8 have been recognized as multifunctional agents, which both activate and repress gene transcription (Antonczyk et al., 2019). The N-terminal DBD and C-terminal IAD are connected by the linker domain (LD), which has been rarely studied (Paul et al., 2018).

IRF9 was discovered as a protein subunit purified from ISGF3 in mammal, which was also known as ISGF3γ or p48 in early studies because of its molecular weight of 48 kDa (Fu et al., 1990). Early study identified that IRF9 played an important role as an interferon-stimulated response element (ISRE)-binding and recognizing protein and the combination with STAT1-STAT2 heterodimers added to its specificity for the ISRE (Kraus et al., 2003). The subsequential study revealed that the acetylation of IRF9 at residue Lys81 was required for its DNA binding activity in U2A cells (Tang et al., 2007). IRF9 has also been found to be involved in cell death pathway in humans, in which overexpression of IRF9 facilitated the antiproliferative activity of IFNα (Tsuno et al., 2009). Recent evidence has indicated that IRF9 is also involved in NF-κB pathway in humans, in which overexpression of IRF9 and U-STAT2 (STAT2 lacking tyrosine phosphorylation) greatly enhances IL6 expression in response to the classical NF-κB activators LPS, TNF, and IL1 (Nan et al., 2018). In teleost, IRF9 has been cloned and characterized from several species, such as crucian carp (*Carassius auratus*), zebrafsh (*Danio rerio*), spotted green pufferfish (*Tetraodon nigroviridis*), Atlantic salmon (*Salmo salar*), olive flounder (*Paralichthys olivaceus*), miiuy croaker (*Miichthys miiuy*) and grass carp (*Ctenopharyngodon idella*) (Shi et al., 2012; Sobhkhez et al., 2014; Hu et al., 2014; Wu et al., 2017). Most of these studies mainly focused on the relationship between STAT2 and IRF9 in the innate immunity (Shi et al., 2012; Wu et al., 2017; Huang et al., 2017). However, there are few studies about the STAT1 and IRF9 in teleost, although the combination of IRF9 and STAT1 is essential for the stability and transcriptional activity of ISGF3 in humans and mammals (Paul et al., 2018).

Black carp is an economically important freshwater species in China, which is subjected to bulk of pathogenic microorganisms, such as GCRV. However, its innate immune system remains largely unknown. In our previous study, bcIRF3, bcIRF5 and bcIRF7 have been investigated separately, with all shown to be involved in regulating antiviral immune response (Jiang et al., 2019; Yang et al., 2019; Li et al., 2018). In this paper, we have reported the full-length cDNA sequence of black carp IRF9 and characterized its structures and features. In addition, two members of STAT1 of black carp (bcSTAT1), bcSTAT1a and bcSTAT1b, have been cloned and characterized to play an important role in the innate immune activation initiated by GCRV (Wu et al., 2019). It was interesting that human STAT1α/β are generated by alternative splicing; however, bcSTAT1a/b isoforms are derived from two different genes (Song et al., 2011). To further explore the mechanism of bcSTAT1a/b in the antiviral innate immunity, the function of bcIRF9 has been identified in this study. bcIRF9 showed strong ISRE-inducing ability and antiviral activity in reporter assay and plaque assay respectively. It was interesting that the ISRE-inducing ability and antiviral activity of IRF9 were obviously elevated by bcSTAT1a, however, dampened by bcSTAT1b, which lacks a complete transcriptional activation domain (TAD) at the C-terminus compared to STAT1a. Thus, our data presented for the first time that STAT1 members function differently in IRF9 regulation, which sheds a light on the STAT1/STAT2/IRF9 study in teleost.

## 2. Materials and methods

### 2.1. Cells and plasmids

HEK293T cells were kept in the lab, *Epithelioma papulosum cyprinid* (EPC) cells and *Ctenopharyngodon idella* kidney (CIK) cells were kind gifts from Dr. Pin Nie (Institute of Hydrobiology, CAS), and *Mylopharyngodon piceus* kidney (MPK) cells were a kind gift from Dr. Tiansheng Chen (Huazhong Agricultural University) (Zhou et al., 2015). All the cell lines were maintained in DMEM supplemented with 10% fetal bovine serum, 2 mM L-glutamine, 100 U/ml penicillin and 100 μg/ml streptomycin. Mammalian cells were cultured at 37 °C with 5% $CO_2$ and fish cells were cultured at 26 °C with 5% $CO_2$. Transfection was done as previously described, calcium phosphate was used for HEK293T transfection and Lipomax (SUDGEN) was used for EPC transfection (Xiao et al., 2017).

pcDNA5/FRT/TO (Invitrogen), pcDNA5/FRT/TO-bcSTAT1a-HA, pcDNA5/FRT/TO-bcSTAT1b-HA and pRL-TK were kept in the lab (Liu et al., 2017). Luci-ISRE was a kind gift from Dr. Yongan Zhang (Huazhong Agriculture University), which contained five ISRE motifs in series (Li et al., 2014). The recombinant vector pcDNA5/FRT/TO-Flag-bcIRF9 was constructed by cloning the open reading frame (ORF) of bcIRF9 fused with a Flag tag at its N-terminus into pcDNA5/FRT/TO.

### 2.2. Cloning the cDNA of bcIRF9

Primers (Table 1) were designed to amplify the coding sequence (CDS) of bcIRF9 based on the transcriptome data of black carp. Total RNA was isolated from the spleen of black carp by Trizol (TaKaRa, Japan) and the first-strand cDNA were synthesized by using the Revert Aid First Strand cDNA Synthesis Kit (Thermo, USA). The coding sequence was cloned at the first attempt by using the primers. The amplified fragments were cloned into pMD18-T vector (TaKaRa, Japan) and sequenced by Invitrogen.

### 2.3. Virus produce and titration

GCRV (strain: GCRV106) were kept in the lab. GCRV were propagated in CIK at 26 °C in the presence of 2% fetal bovine serum. Virus titers were determined by plaque assay on EPC cells separately as previously described (Jiang et al., 2017). Briefly, the 10-fold serially diluted virus supernatants were added onto EPC cells and incubated for 2 h at 26 °C. The supernatant was removed after incubation and DMEM

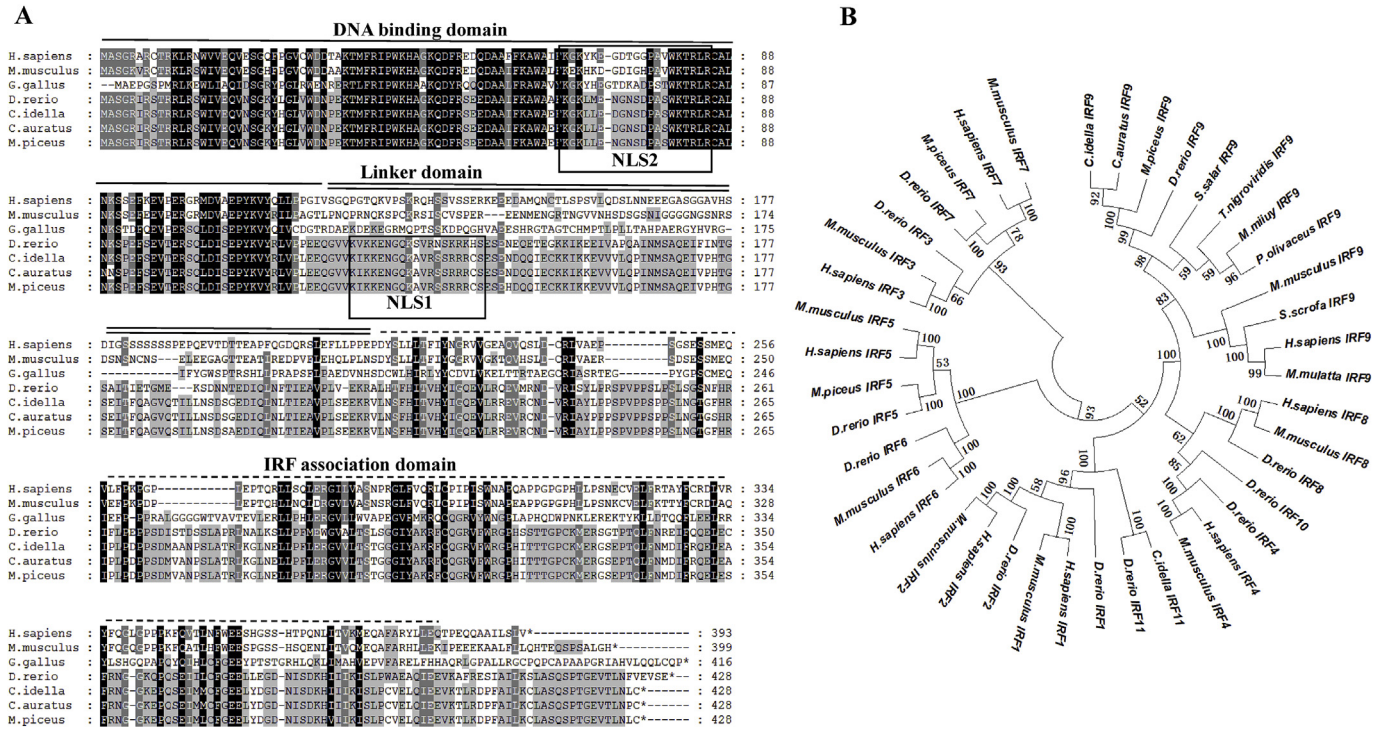


**Fig. 1.** Evolution study of bcIRF9.

(A): Comparisons of bcIRF9 with other vertebrate IRF9 proteins by using MEGA 6.0 program and GeneDoc program. The N-terminal DNA binding domain, C-terminal IRF association domain and middle linker domain were labeled above the sequences. Two nuclear location domains (NLS1 and NLS2) were indicated with rectangle separately. The domains were predicted by CDS (Conserved Domain Search) of NCBI (https://www.ncbi.nlm.nih.gov/Structure/cdd/wrpsb.cgi). Nuclear location domains were predicted by PSORT II (https://psort.hgc.jp/form2.html). (B): Phylogenetic tree of IRFs in vertebrates. The tree was depicted on the overall sequences by neighbor-joining method of MEGA 6.0 software. The accession numbers of the IRF1 sequences are: *H. sapiens* (CR541713.1), *M. musculus* (BC003821.1), *D. rerio* (AY398364.1). The accession numbers of the IRF2 sequences are: *H. sapiens* (CR457077.1), *M. musculus* (BC006577.2), *D. rerio* (BC086813.1). The accession numbers of the IRF3 sequences are: *H. sapiens* (AAH09395.1), *M. musculus* (NP_001006970), *D. rerio* (NP_001137376.1). The accession numbers of the IRF4 sequences are: *H. sapiens* (CAH71554.1), *M. musculus* (AK089319), *D. rerio* (NP_001116182.1). The accession numbers of the IRF5 sequences are: *H. sapiens* (EAL24107.1), *M. musculus* (EDL13770.1), *M. piceus* (MK422172.1), *D. rerio* (ABY91289.1). The accession numbers of the IRF6 sequences are: *H. sapiens* (AEL89176.1), *M. musculus* (NM_016851.2), *D. rerio* (AAH56772.1). The accession numbers of the IRF7 sequences are: *H. sapiens* (BC136555.1), *M. musculus* (BC138799.1), *M. piceus* (MG210943.1), *D. rerio* (BC065902.1). The accession numbers of the IRF8 sequences are: *H. sapiens* (NP_002154.1), *M. musculus* (NM001008722), *D. rerio* (NM_001002622.1). The accession numbers of the IRF9 sequences are: *M. mulatta* (NP_001260669.1), *H. sapiens* (006084.4), *M. musculus* (BC005435.1), *S. scrofa* (NM_001078670.1), *S. salar* (NM_001173719.1), *C. auratus* (JQ804926.1), *D. rerio* (NM_001260669.1), *C. idella* (KT156366.1), *M. piceus* (MH410168.1), *M. miiuy* (KY091659.1), *L. crocea* (MF446411.1), *T. nigroviridis* (JQ412058.1). The accession numbers of the IRF10 sequences are: *D. rerio* (NP_998044.1). The accession numbers of the IRF11 sequences are: *D. rerio* (BC165272.1), *C. idella* (MH797556.1). The bar stands for the scale length and the numbers on different nodes stand for bootstrap value.

**Table 2**
Comparison of bcIRF9 with other vertebrate IRF9 (%).

| Species | Full-length sequence | |
|---|---|---|
| | Similarity | Identity |
| *C.idella* | 99.5 | 97.9 |
| *C.auratus* | 98.8 | 97.2 |
| *D.rario* | 85.4 | 76.9 |
| *S.salar* | 70.5 | 55.2 |
| *M.milluy* | 69.1 | 54.9 |
| *T.nigrovirids* | 66.4 | 52.3 |
| *P.olivaceus* | 66.4 | 52.2 |
| *L.crocea* | 58.8 | 46.6 |
| *G.gallus* | 46.2 | 33.5 |
| *H.sapiens* | 47.6 | 33.1 |
| *M.mulatta* | 47.1 | 33.6 |
| *S.scrofa* | 45.3 | 32.1 |
| *M.musculus* | 47.4 | 33.3 |
| *M.fascicularis* | 18.5 | 31.4 |

The protein IDs are identical to those of Fig. 1.

containing 2% FBS and 0.75% methylcellulose (Sigma) was added. Plaques were counted at day 3 post infection.

### 2.4. Quantitative real-time PCR

The relative bcIRF9 mRNA level in MPK cells was examined by quantitative real-time PCR (q-PCR). The primers for bcIRF9 and β-actin (as internal control) were listed in Table 1. The q-PCR program was: 1 cycle of 95 °C/10min, 40 cycles of 95 °C/15s, 60 °C/1min, followed by dissociation curve analysis (60 °C–95 °C) to verify the amplification of a single product. The threshold cycle (CT) value was determined by using the manual setting on the 7500 Real-Time PCR System and exported into a Microsoft Excel Sheet for subsequent data analysis where the relative expression ratio of target gene of treated group versus that of control group were calculated by $2^{-\triangle\triangle CT}$ method.

### 2.5. LPS and poly (I:C) treatment

MPK cells were seeded in 6-well plate ($2 \times 10^6$ cells/well) at 16 h before treatment. poly (I:C) (Sigma) was used for synthetic dsRNA stimulation, which was heated to 55 °C (in PBS) for 5min and cooled at room temperature before use. MPK cells were replaced with 1 ml fresh

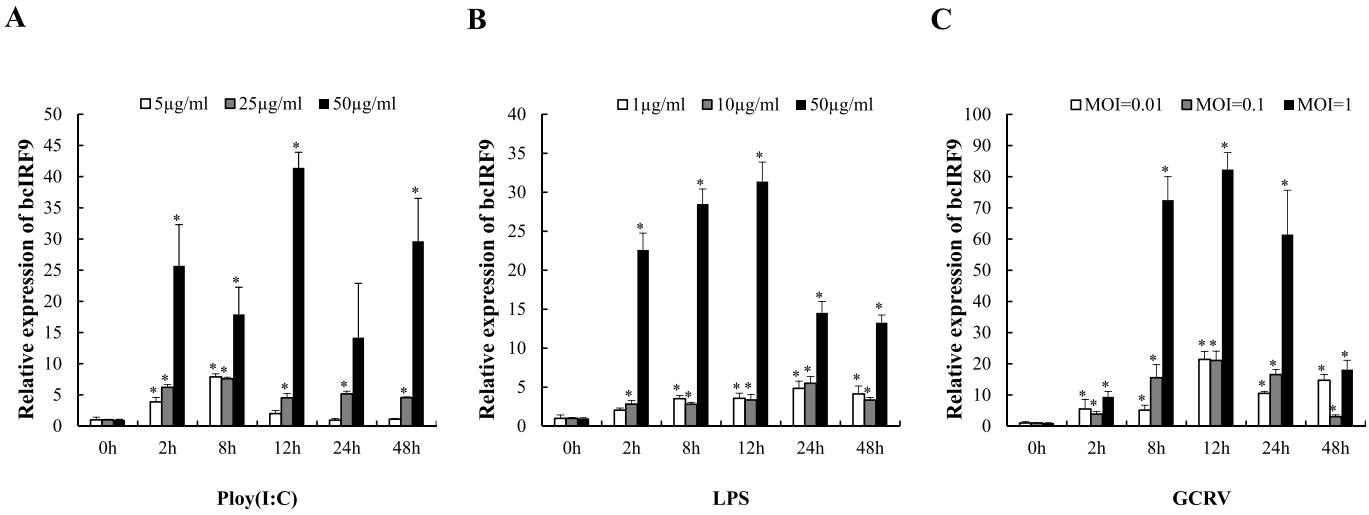


**Fig. 2.** The expression of bcIRF9 in response to different stimuli.
MPK cells were seeded in 6-well plate ($2 \times 10^6$ cells/well) at 16 h before stimulation. The cells were treated with poly (I:C) or LPS at the indicated concentrations (A& B) or infected with GCRV at indicated MOIs separately (C), and harvested for qPCR independently at the indicated time points post stimulation.

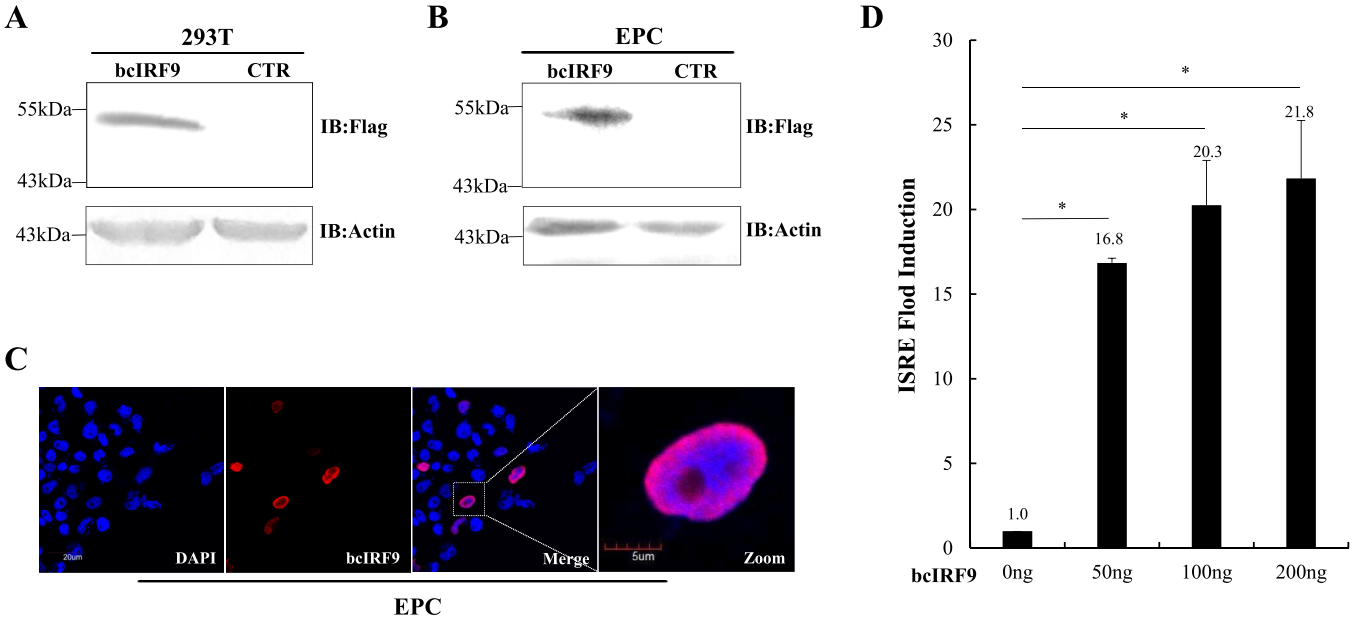


**Fig. 3.** The protein expression, subcellular distribution and ISRE-inducing ability of bcIRF9.
(A) & (B) Immunoblot assay of bcIRF9 in 293T cells and EPC cells. CTR: cells transfected with empty vector, IB: immunoblot. (C): Immunofluorescence staining of bcIRF9 in EPC cells; the bar stands for the scale of 20 μm and 5 μm respectively. (D): EPC cells in 24-well plate were transfected with plasmid expressing bcIRF9, pRL-TK and Luci-ISRE and applied to reporter assay. The numbers above the error bars stand for the average ISRE fold induction. bcIRF9: pcDNA5/FRT/TO-Flag-bcIRF9.

media containing poly (I:C) and harvested at different time points post treatment. For LPS treatment, MPK cells in 6-well plate ($2 \times 10^6$ cells/well) were treated with LPS at indicated concentration and harvested for q-PCR at different time point post stimulation as above.

### 2.6. Immunoblotting

EPC cells in 6-well plate ($2 \times 10^6$ cells/well) were transfected with pcDNA5/FRT/TO-Flag-bcIRF9 or the empty vector separately. The transfected cells were harvested at 48 h post transfection and the whole cell lysates were used for immunoblot (IB) assay as previously described (Yang et al., 2019). In brief, the proteins were isolated by 10% SDS-PAGE and the transferred membrane was probed with mouse-anti-Flag monoclonal antibody (1:4000; Sigma, USA), which was followed by the incubation with goat anti-mouse IgG (1:30000; Sigma, USA). The target protein was visualized with BCIP/NBT alkaline phosphatase color development kit (Thermo, USA).

### 2.7. Immunofluorescence microscopy

EPC cells in 24-well ($3 \times 10^5$ cells/well) plate were transfected with pcDNA5/FRT/TO-Flag-bcIRF9, and/or pcDNA5/FRT/TO-bcSTAT1a-HA or pcDNA5/FRT/TO-bcSTAT1b-HA. The transfected cells were fixed with 4% (v/v) paraformaldehyde at 24 h post transfection. The fixed cells were permeabilized with Triton X-100 (0.2% in PBS) and used for immune-fluorescent staining as previously described (Li et al., 2019). Rabbit-anti-HA antibody and mouse-anti-Flag antibody (Sigma, USA) were probed at the ratio of 1:300. Alexa 594-conjugated secondary antibody (Invitrogen, USA) and Alexa 488-conjugated secondary antibody (Invitrogen, USA) were probed at the ratio of 1:1000; and DAPI (4,

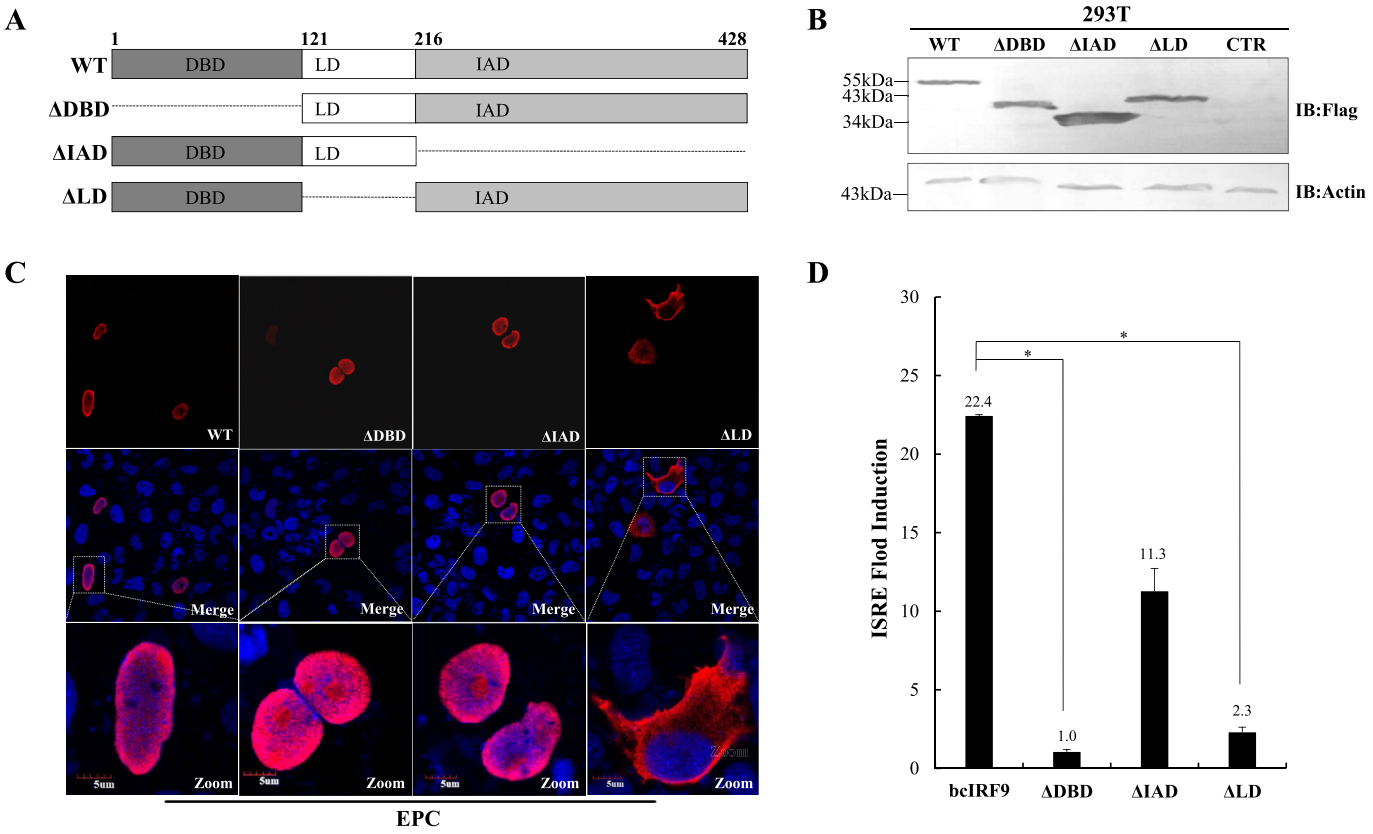


**Fig. 4.** The protein expression, subcellular distribution and ISRE-inducing ability of the truncation mutants of bcIRF9.
(A): Schematic map of bcIRF9 and its truncation mutants. (B): Immunoblot assay of bcIRF9 and its mutants in 293T cells. CTR: cells transfected with the empty vector, IB: immunoblot. (C): Immunofluorescence staining of bcIRF9 and its mutants in EPC cells. The bar stands for the scale of 5 μm. (D): EPC cells in 24-well plate were transfected with bcIRF9 or its mutants, and applied to reporter assay. WT: pcDNA5/FRT/TO-Flag-bcIRF9; ΔDBD: pcDNA5/FRT/TO-Flag-ΔDBD-bcIRF9; ΔIAD: pcDNA5/FRT/TO-Flag-ΔIAD-bcIRF9; ΔLD: pcDNA5/FRT/TO-Flag-ΔLD- bcIRF9. The numbers above the error bars stand for the average ISRE fold induction.

6-diamidino-2-phenylindole) were used for the nucleus staining.

### 2.8. Luciferase reporter assay

EPC cells in 24-well plate ($3 \times 10^5$ cells/well) were co-transfected with expression plasmids as required, pRL-TK and Luci-ISRE. For each transfection, the total amount of DNA was balanced with the empty vector. The cells were harvested and lysed at 24 h post transfection. The centrifuged supernatant was used to measure the activities of firefly luciferase and renilla luciferase according to the instruction of the manufacturer (Promega, USA) as previously described (Song et al., 2019).

### 2.9. Co-immunoprecipitation (Co-IP)

HEK293T cells in 10 cm Petri dish ($6 \times 10^6$ cells/well) were co-transfected with pcDNA5/FRT/TO-Flag-bcIRF9 and pcDNA5/FRT/TO-bcSTAT1a-HA or pcDNA5/FRT/TO-bcSTAT1b-HA separately. For each transfection, the total amount of plasmid DNA was balanced with the empty vector. The transfected cells were harvested at 48 h post-transfection and lysed for immunoprecipitation (IP) assay as previously described (Lu et al., 2017). The whole cell lysate of the transfected cells was incubated with protein A/G agarose beads at 4 °C for 2 h. Anti-Flag-conjugated protein A/G agarose beads were added in the supernatant after pre-cleaning and incubated with the supernatant media at 4 °C for 4 h. The anti-Flag-conjugated protein A/G agarose beads were boiled in 2 × sample buffer after 3 times of wash and the eluted proteins were used for IB as above.

### 2.10. Statistics analysis

For the statistics analysis in q-PCR, luciferase reporter assay and viral titer measurement, all data were obtained from three independent experiments with each performed in triplicate. Error bars represented the standard error of the mean value (+SEM) of three independent experiments. Asterisks (*) on the pillar marked the significant difference between experimental data and control data (*$p < 0.05$). The data were analyzed by two-tailed Student's t-test.

## 3. Results

### 3.1. Molecular cloning and sequence analysis of bcIRF9

The CDS of *bcIRF9* consists of 1287 nucleotides, which encodes 428 amino acids (NCBI accession number: MH410168.1). The sequence analysis predicts that bcIRF9 contains a highly conserved N-terminal DNA binding domain (DBD), a linker domain (LD), and an IRF associated domain (IAD). A previous report has showed that human IRF9 contains a bipartite NLS (named as NLS2) motif at the position of 66aa-85aa. Multiple sequence alignments revealed that the NLS2 domain is highly conserved in the corresponding region of all selected IRF9 proteins from human to fish (Fig. 1A). In addition, the PSORTII software predication and sequence alignment have revealed that bcIRF9 possesses a fish-specific nuclear localization signal (NLS1) like its piscine homologues (Fig. 1A). The calculated molecular weight of bcIRF9 is 48.31 kDa and the theoretical isoelectric point of this protein is 7.98 (http://web.expasy.org/protparam/). Phylogenetic analysis has shown

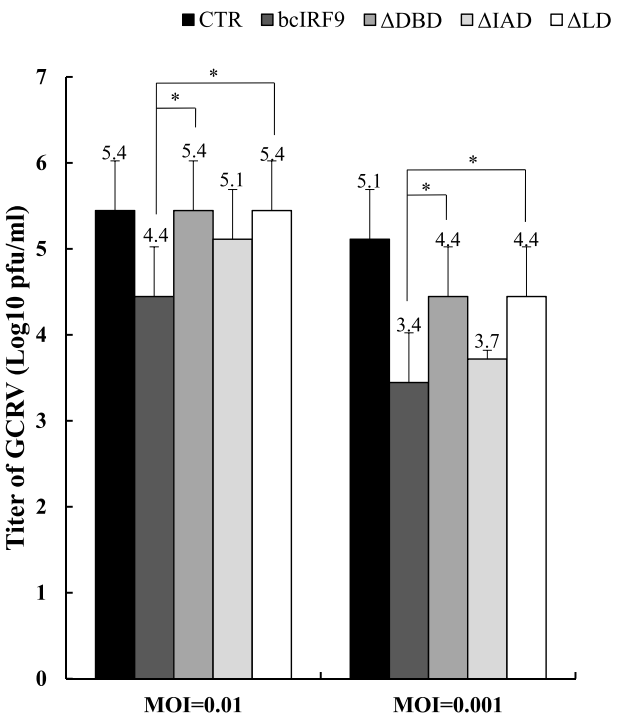


**Fig. 5.** The antiviral activity of bcIRF9 and its mutants.
EPC cells in 24-well plate were transfected with 500 ng plasmids expressing bcIRF9, its mutants or the empty vector separately. At 24 h post transfection, cells were infected with GCRV at the indicated MOI. The virus titers in the supernatant media were examined by plaque assay at 24 hpi. CTR: EPC cells transfected with the empty vector; bcIRF9: pcDNA5/FRT/TO-Flag-bcIRF9; ΔDBD: pcDNA5/FRT/TO- Flag-ΔDBD-bcIRF9; ΔIAD: pcDNA5/FRT/TO-Flag-ΔIAD-bcIRF9; ΔLD: pcDNA5/FRT/TO-Flag-ΔLD-bcIRF9. The numbers above the error bars stand for average virus titer.

that black carp IRF9 is orthologous to mammalian counterparts, which grouped with IRF4, IRF8, and IRF10 proteins constituting the IRF4 subfamily (Fig. 1B). bcIRF9 shares high amino acid sequence similarity with grass carp IRF9 (99.5%) and crucian carp IRF9 (98.8%), which correlates with the closest genetic relationship of these cyprinid fishes (Table 2).

### 3.2. bcIRF9 expression in response to different stimuli

To learn bcIRF9 mRNA profile during the innate immune activation, MPK cells were subjected to different stimuli and applied to qPCR analysis, which including poly (I:C), LPS and GCRV. After poly (I:C) stimulation, the transcription of bcIRF9 immediately increased right after stimulation and the trends were same in all groups treated at different concentration (5 μg/ml, 25μg/ml or 50μg/ml) and the overall trend of the transcription of bcIRF9 were initially elevated and then decreased (Fig. 2A). The highest transcription level of bcIRF9 (12 h point, 50μg/ml) within 48 h post stimulation was up to 41.4-fold of that of the control (Fig. 2A). Similar to that of poly (I:C) group, the transcription of bcIRF9 in MPK cells was increased right after LPS treatment and the highest transcription level of bcIRF9 (12 h point, 50μg/ml) within 48 h post stimulation was up to 31.4-fold of that of the control (Fig. 2B). In GCRV infected MPK cells, the transcription of bcIRF9 was increased right after virus infection and the trends of bcIRF9 transcription were similar in all groups (0.01, 0.1 and 1 MOI). The highest transcription level of bcIRF9 (12 h point, 1 MOI) within 48 h post infection (hpi) was up to 82.3-fold of that of the control (Fig. 2C). These data implied that bcIRF9 was involved in host innate immune response against virus and bacteria.

### 3.3. Protein expression and subcellular distribution of bcIRF9

Both HEK293T cells and EPC cells were transfected with plasmids expressing bcIRF9 and used for IB assay to investigate the protein expression of bcIRF9. A specific band of ~54 kDa was detected in the whole cell lysate of both HEK293T and EPC cells expressing bcIRF9, but not in the control groups (Fig. 3A&B). bcIRF9 migrated a little heavier (54 kDa) than its predicted molecular size (48.31 kDa) in the IB of both mammalian cells and fish cells, which might be explained by that there existed a proline-rich area in bcIRF9 (247aa-272aa). And similar phenomenon was seen in the IB data of black carp MAVS (bcMAVS), which also possessed a proline-rich area (Zhou et al., 2015). To determine the subcellular distribution of bcIRF9, EPC cells were transfected with plasmids expressing bcIRF9 and analyzed by immunofluorescence (IF) staining assay. In the IF data of bcIRF9, the brilliant red color representing bcIRF9-expressing area was detected in nucleus of EPC cells (Fig. 3C). The IF data suggested that bcIRF9 distributed predominantly in the nucleus like its mammalian counterpart (Lau et al., 2000).

To investigate the function of the domains of bcIRF9, plasmids expressing ΔDBD-bcIRF9 (bcIRF9 without DBD domain), ΔIAD-bcIRF9 (bcIRF9 without IAD domain), ΔLD-bcIRF9 (bcIRF9 without LD domain) were generated separately (Fig. 4A). IB data demonstrated that wild type bcIRF9 and the bcIRF9 truncates were well expressed in HEK293T cells (Fig. 4B). The subcellular localizations of bcIRF9 truncates were examined by IF staining, which was aimed to identify the crucial domain for nuclear localization of this protein. Both ΔDBD-bcIRF9 and ΔIAD-bcIRF9 were expressed predominantly in the nucleus; however, ΔLD-bcIRF9, unlike the wild type bcIRF9, was mainly distributed in the cytosol part (Fig. 4C). The IF data demonstrated that linker domain (LD) of bcIRF9 was indispensable for its nuclear localization.

### 3.4. The antiviral signaling mediated by bcIRF9

To determine the ISRE-inducing activity of bcIRF9, EPC cells were transfected with plasmids expressing bcIRF9 or its truncates, and applied to dual luciferase reporter assay. The ISRE fold induction increased as well as the bcIRF9 input increased (50 ng, 100 ng, 200 ng), which clearly demonstrated the expression of bcIRF9 in EPC cells induced the transcription of ISRE (Fig. 3D). As to the bcIRF9 truncates, ΔIAD-bcIRF9 still possessed the ISRE-inducing activity, which was although not as strong as that of wile type bcIRF9. However, ΔDBD-bcIRF9 and ΔLD-bcIRF9 showed little effect on the activation of ISRE (Fig. 4D), which demonstrated that DBD and LD were indispensable for bcIRF9-induced ISRE activation. To test the antiviral activity of bcIRF9, EPC cells were transfected with plasmids expressing bcIRF9, ΔDBD-bcIRF9, ΔIAD-bcIRF9 or ΔLD-bcIRF9 separately before subjected to GCRV infection. The plaque assay data demonstrated that EPC cells expressing wild type bcIRF9 or ΔIAD-bcIRF9 obtained enhanced antiviral activity against GCRV compared with the control cells, in which EPC cells expressing bcIRF9 presented stronger antiviral activity than EPC cells expressing ΔIAD-bcIRF9. However, EPC cells expressing either ΔDBD-bcIRF9 or ΔLD-bcIRF9 showed similar antiviral activity to that of the control cells (Fig. 5), which correlated with the reporter assay data (Fig. 4D). Taken together, reporter assay data and plaque assay data demonstrated that both DBD and LD were crucial for bcIRF9-mediated antiviral signaling.

### 3.5. The relation between bcSTAT1 and bcIRF9

In teleost, little is known about the role of STAT1 in IRF9-mediated antiviral signaling, which led us to explore the relationship between bcSTAT1 and bcIRF9. The previous data has demonstrated that two bcSTAT1 members, bcSTAT1a and bcSTAT1b, play important roles in the innate immunity (Wu et al., 2019). In the reporter assay, both STAT1a and STAT1b showed little ISRE-inducing activity when they

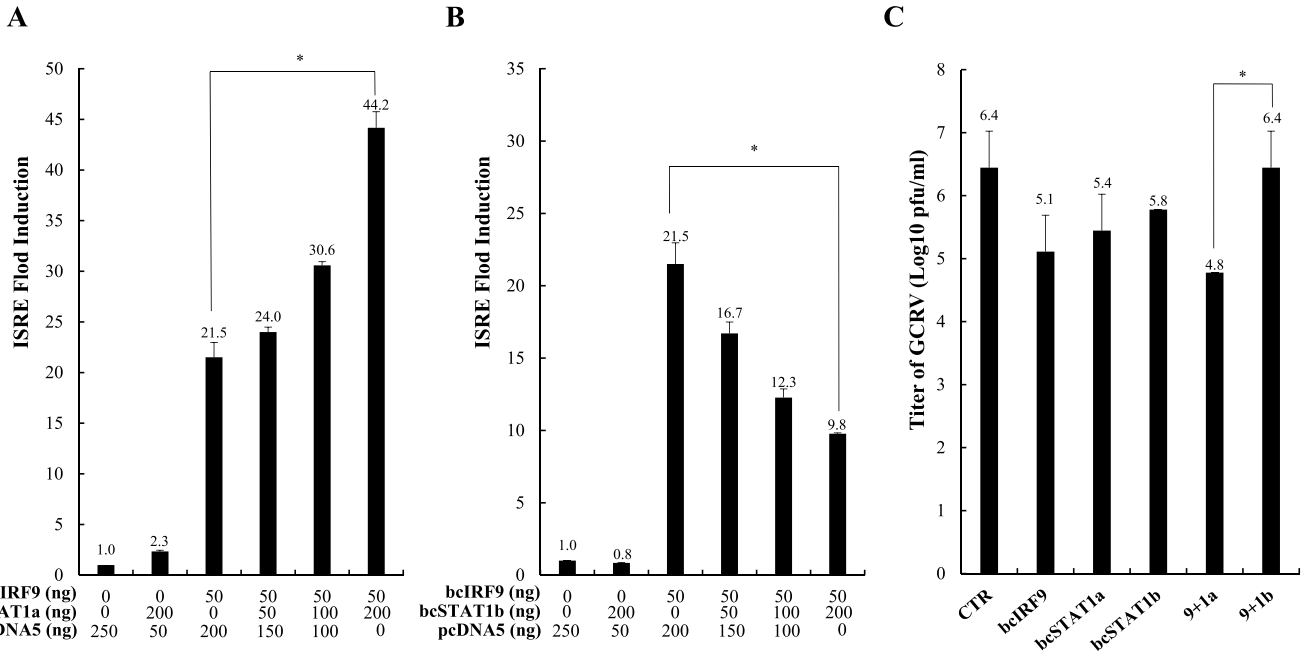


**Fig. 6.** The role of bcSTAT1a and bcSTAT1b in bcIRF9-mediated ISRE activity.
(A&B): EPC cells in 24-well plate were co-transfected with plasmids expressing bcIRF9 and bcSTAT1a (or bcSTAT1b), and applied to reporter assay. pcDNA5: pcDNA5/FRT/TO; bcIRF9: pcDNA5/FRT/TO-Flag-bcIRF9; bcSTAT1a: pcDNA5/FRT/TO-bcSTAT1a-HA; bcSTAT1b: pcDNA5/FRT/TO-bcSTAT1b-HA. The numbers above the error bars stand for the average ISRE fold induction. (C): EPC cells in 24-well plate were transfected with bcIRF9 and/or bcSTAT1a (or bcSTAT1b); and then infected with GCRV (MOI = 0.1) at 24 h post transfection. The virus titers in the supernatant media were examined by plaque assay at 24 hpi. CTR: pcDNA5/FRT/TO; bcIRF9: pcDNA5/FRT/TO-Flag-bcIRF9; bcSTAT1a: pcDNA5/FRT/TO-bcSTAT1a-HA; bcSTAT1b: pcDNA5/FRT/TO-bcSTAT1b-HA; 9 + 1a: pcDNA5/FRT/TO-Flag-bcIRF9 and pcDNA5/FRT/TO-bcSTAT1a-HA; 9 + 1b: pcDNA5/FRT/TO-Flag-bcIRF9 and pcDNA5/FRT/TO-bcSTAT1b-HA. The numbers above the error bars stand for average virus titer.

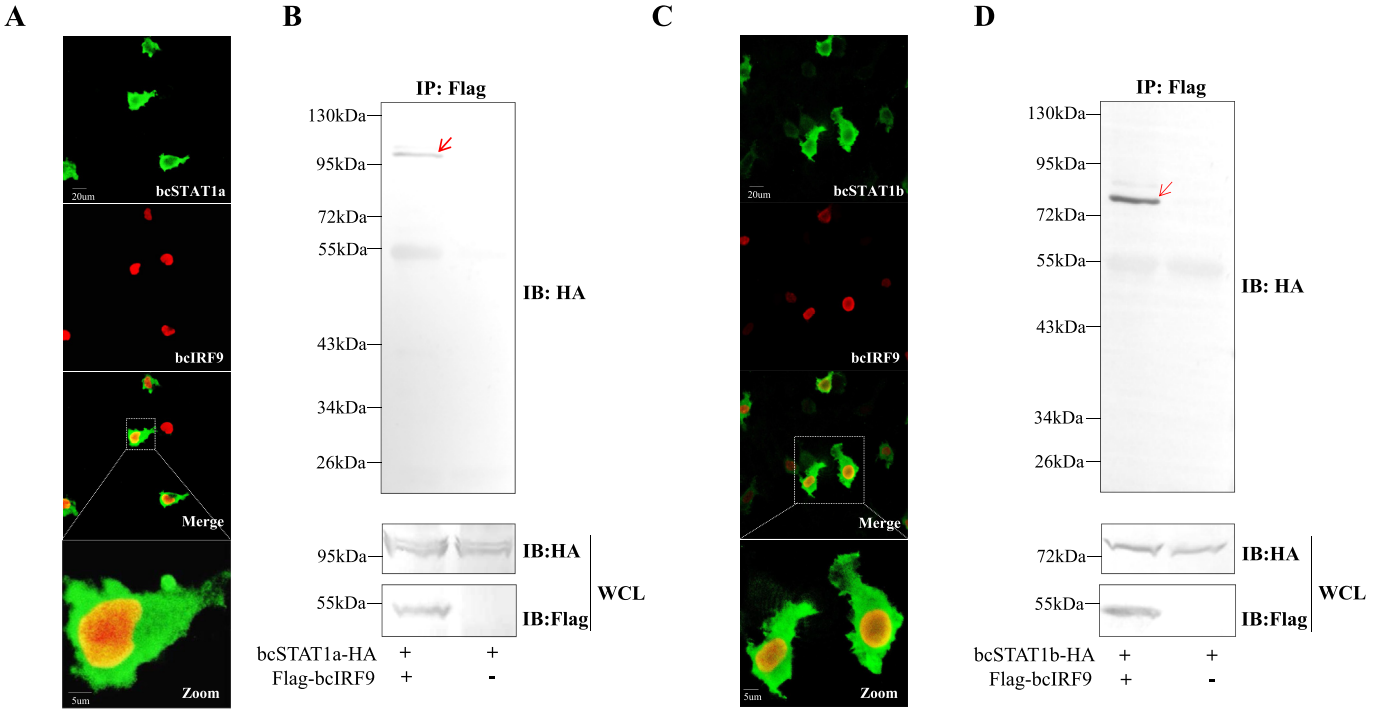


**Fig. 7.** The association between bcIRF9 and bcSTAT1.
(A&C): Immunofluorescence staining of EPC cells co-expressing bcIRF9 and bcSTAT1a (or bcSTAT1b). bcIRF9: pcDNA5/FRT/TO-Flag-bcIRF9; bcSTAT1a: pcDNA5/FRT/TO-bcSTAT1a-HA; bcSTAT1b: pcDNA5/FRT/TO-bcSTAT1b-HA. The bars stand for the scale of 20 μm and 5 μm accordingly. (B&D): Co-IP in HEK293T cells between bcIRF9 and bcSTAT1a-HA (or bcSTAT1b). IB:immunoblot; IP: immunoprecipitation; WCL: whole cell lysate; Flag-bcIRF9: pcDNA5/FRT/TO-Flag-bcIRF9; bcSTAT1a-HA: pcDNA5/FRT/TO-bcSTAT1a-HA; bcSTAT1b-HA: pcDNA5/FRT/TO-bcSTAT1b-HA.

were expressed alone in EPC cells. In EPC cells co-expressing bcSTAT1a and bcIRF9, co-expressed bcSTAT1a up-regulated bcIRF9-mediated ISRE fold induction in a dose-dependent manner. However, bcIRF9-mediated ISRE fold induction was down-regulated by the co-expressed bcSTAT1b in a dose-dependent manner (Fig. 6A&B). Accordingly, the plaque assay demonstrated that bcIRF9-meidated antiviral activity of EPC cells against GCRV was up-regulated by bcSTAT1a and down-regulated by bcSTAT1b (Fig. 6C). Our previous data has demonstrated that bcSTAT1a and bcSTAT1b were distributed in both cytosol and nucleus (Wu et al., 2019). The IF data in this paper showed that co-expression of bcSTAT1 and bcIRF9 did not change the nuclear distribution of these proteins, and bcIRF9-expressing region (red color) matched that of bcSTAT1a/b-expressing region (green color, nuclear part), which implied the potential interaction between bcIRF9 and bcSTAT1 (Fig. 7A and C). The sub-sequential co-immunoprecipitation assay showed clearly that both bcSTAT1a and bcSTAT1b were detected in the bcIRF9-precipitated proteins, which identified the direct association between bcIRF9 and bcSTAT1a/b (Fig. 7B and D).

## 4. Discussion

IRFs are critical for the innate and adaptive immunity by regulating the transcription of IFNs and IFN-induced gene expression in vertebrates (Antonczyk et al., 2019). As a key member of IRF family, IRF9 have been investigated in many species from human to teleost. In mammals, IRF9 has been recognized as a DNA-binding adapter protein of IFN stimulated gene factor 3 (ISGF3) in the JAK-STAT signaling (Paul et al., 2018). There is a growing interest in teleost IRF9 study on its broad impact on the antiviral immunity. Crucian carp IRF9 has been reported to be able to induce the expression of IFN and ISG (Shi et al., 2012). In the studies of miiuy croaker and Japanese flounder, the mRNA variation of IRF9 can be detected in tissues of fish injected with poly I:C or lymphocystis disease virus (LCDV) (Hu et al., 2014; Yang et al., 2017). bcIRF9 possesses three conserved domains like its fish and mammalian counterparts and two nuclear location signals (NLS), NLS1 and NLS2, (Fig. 1A). NLS2 is highly conservative from mammal to fish; however, NLS1 is unique among all fish IRF9 members, which is located in the LD and composed of a stretch of lysines (K) and arginines (R) (Shi et al., 2008). The IF data of bcIRF9 truncation mutants showed clearly that ΔLD-bcIRF9, unlike the wild type bcIRF9, ΔDBD-bcIRF9 or ΔIAD-bcIRF9, was distributed in the cytosol (Fig. 4C). Thus, our data demonstrates that NLS1 is crucial for the nuclear location of bcIRF9 and is different to that of crucian carp IRF9 (Shi et al., 2012), in which both NLS1 and NLS2 are necessary for the nuclear localization of crucian carp IRF9. NLS1 of bcIRF9 shares 100% identity to that of crucian carp IRF9; however, NLS2 of bcIRF9 presents one amino acid difference ($N_{72}$) to that of crucian carp IRF9 ($D_{72}$), which implies this aspartic acid (D) is crucial for the predicted NLS2 of crucian carp IRF9. ΔDBD-bcIRF9 and ΔLD-bcIRF9 showed fiercely decreased ISRE-inducing ability and antiviral activity compared with the wild type bcIRF9, suggested that both the DNA binding activity and the nuclear accumulation of bcIRF9 were crucial for its mediated antiviral signaling (Figs. 4D and 5), which was similar to its mammalian counterpart (Cheon et al., 2013).

STAT proteins belong to a family of transcription factors, which are activated by a number of cytokines and growth factors (Gao et al., 2012). After the translocation from the cytoplasm to the nucleus, the activated STATs bind to the specific promoter elements of target genes and regulate their transcription (Blaszczyk et al., 2016). The diversity and specificity of the JAK-STAT signal transduction pathway have been increased by STAT isoforms, which are derived from differential splicing of STATs mRNA and posttranslational proteolytic processing of STATs (Lim and Cao, 2006). Although the shorter isoforms of STATs lack a functional transcriptional activation domain, they still remain the DNA-binding ability specific for the promoters of target genes, which inhibit the transcription of target genes through competing with full length STATs for DNA binding sites (Palosaari et al., 2003).

As a canonical STATs member, STAT1 is a key component the JAK-STAT signaling cascade and play an essential role in mediating responses to all types of IFNs (Meissl et al., 2017). Human STAT1 (HsSTAT1) two splice variants, named STAT1-alpha (HsSTAT1α) and STAT1-beta (HsSTAT1β) separately. Both HsSTAT1α and HsSTAT1β contain six domains; however, HsSTAT1α but not HsSTAT1β contains complete transcription activation domain (TAD) (Zhang et al., 2017). The phosphorylation, DNA binding and transcriptional activity of HsSTAT1α were inhibited by HsSTAT1β in B-cells (Baran-Marszak et al., 2004). To our knowledge, only a single *STAT1* gene has been cloned in teleost fishes except zebrafish and black carp (Song et al., 2011; Wu et al., 2019). Human STAT1 isoforms (HsSTAT1α/β) are generated from one gene through alternative splicing; however, both black carp STAT1 isoforms (bcSTAT1a/b) and Zebrafish STAT1 isoforms (DrSTAT1a/b) are derived from two different genes. bcSTAT1a and DrSTAT1a possesses the complete TAD as HsSTAT1α, but bcSTAT1b and DrSTAT1b contains incomplete TAD as HsSTAT1β. Previous report in zebrafish demonstrated that the expression level of DrSTAT1a and DrSTAT1b had opposite trends with the increase of time after IFN-γ stimulation (Ruan et al., 2017). However, the role of teleost STAT1 isoforms in JAK-STAT signaling remains during host antiviral innate immune activation remains largely unknown.

In this paper, two black carp STAT1 members, bcSTAT1a and bcSTAT1b, have been identified to interact with bcIRF9 (Fig. 7). Both STAT1a and STAT1b showed little effect on the activation of ISRE when they were expressed alone in EPC cells. However, bcIRF9-induced ISRE activation and antiviral activity against GCRV were elevated by bcSTAT1a, but dampened by bcSTAT1b (Fig. 6). It is reasonable that the different roles of STAT1a and STAT1b in regulating IRF9-mediated ISRE signaling in black carp are important for host cells to keep homeostasis when facing pathogens invading. This result implied that bcSTAT1a/b might play a role like “molecular switch” in the JAK-STAT signaling pathway in black carp. After the pathogenic microorganisms invasion, host-derived IFNs induce bcSTAT1a with bcSTAT2 and bcIRF9 to form ISGF3 complex, which subsequentially translocate from cytoplasm to the nucleus to activate the transcription of ISGs to resist invasion. During and after host antiviral innate immune activation, bcSTAT1b might replace bcSTAT1a through uncertain mechanism to prevent host from over-immune disorders. In our previous study, bcSTAT1a and bcSTAT1b transcription increased in response to poly (I:C), LPS and GCRV; however, the mRNA level increase rate of bcSTAT1a was obviously lower than that of bcSTAT1b (Wu et al., 2019). Thus, it is speculated that the invading pathogens, such as GCRV, might “hijack” black carp STAT1b to facilitate its replication.

## Acknowledgements

This work was supported by the National Natural Science Foundation of China (31920103016), Hunan Provincial Education Department (18A011), the Cooperative Innovation Center of Engineering and New Products for Developmental Biology of Hunan Province (20134486) and the Modern Agricultural Industry Program of Hunan Province.

## References

Antonczyk, A.M., Krist, B., Szelag, M., Michalska, A., Piaszyk-Borychowska, A., Plens-Galaska, M., Wesoly, J., Bluyssen, H.A., 2019. Direct inhibition of IRF-dependent transcriptional regulatory mechanisms associated with disease. Front. Immunol. 10, 1176.

Baran-Marszak, F., Feuillard, J., Najjar, I., Le Clorennec, C., Béchet, J.M., Dusanter-Fourt, I., Fagard, R., 2004. Differential roles of STAT1α and STAT1β in fludarabine-induced cell cycle arrest and apoptosis in human B cells. Blood 104 (8), 2475–2483.

Blaszczyk, K., Nowicka, H., Kostyrko, K., Antonczyk, A., Wesoly, J., Bluyssen, H.A., 2016. The unique role of STAT2 in constitutive and IFN-induced transcription and antiviral responses. Cytokine Growth Factor Rev. 29, 71–81.

Cheon, H., Holvey-Bates, E.G., Schoggins, J.W., Forster, S., Hertzog, P., Imanaka, N., Stark, G.R., 2013. IFNβ-dependent increases in STAT1, STAT2, and IRF9 mediate

resistance to viruses and DNA damage. EMBO J. 32 (20), 2751–2763.
Chiang, H.S., Liu, H.M., 2018. Molecular basis of viral inhibition of IRF- and STAT-dependent immune responses. Front. Immunol. 3086.
Fu, X.Y., Kessler, D.S., Veals, S.A., Levy, D.E., Darnell, J.E.J., 1990. ISGF3, the transcriptional activator induced by interferon alpha, consists of multiple interacting polypeptide chains. Proc. Natl. Acad. Sci. 87 (21), 8555–8559.
Gao, B., Wang, H., Lafdil, F., Feng, D., 2012. STAT proteins–key regulators of anti-viral responses, inflammation, and tumorigenesis in the liver. J. Hepatol. 57 (2), 430–441.
Hu, G.B., Zhao, M.Y., Lin, J.Y., Liu, Q.M., Zhang, S.C., 2014. Molecular cloning and characterization of interferon regulatory factor 9 in Japanese flounder, Paralichthys olivaceus. Fish Shellfish Immunol. 39 (2), 138–144.
Huang, B., Qi, Z.T., Xu, Z., Nie, P., 2010. Global characterization of interferon regulatory factor (IRF) genes in vertebrates: glimpse of the diversification in evolution. BMC Immunol. 11 (1), 22.
Huang, C.J., Chou, C.M., Lien, H.W., Chu, C.Y., Ho, J.Y., Wu, Y., Cheng, C.H., 2017. IRF9-Stat2 fusion protein as an innate immune inducer to activate Mx and interferon-stimulated gene expression in zebrafish larvae. Mar. Biotechnol. 19 (3), 310–319.
Ivashkiv, L.B., Donlin, L.T., 2014. Regulation of type I interferon responses. Nat. Rev. Immunol. 14 (1), 36–49.
Jiang, S., Xiao, J., Li, J., Chen, H., Wang, C., Feng, C., Feng, H., 2017. Characterization of the black carp TRAF6 signaling molecule in innate immune defense. Fish Shellfish Immunol. 67, 147–158.
Jiang, Y., Liu, L., Yang, S., Cao, Y., Song, X., Xiao, J., Feng, H., 2019. Black carp PRMT6 inhibits TBK1-IRF3/7 signaling during the antiviral innate immune activation. Fish Shellfish Immunol. 93, 108–115.
Kraus, T.A., Lau, J.F., Parisien, J.P., Horvath, C.M., 2003. A hybrid IRF9-STAT2 protein recapitulates interferon-stimulated gene expression and antiviral response. J. Biol. Chem. 278 (15), 13033–13038.
Lau, J.F., Parisien, J.P., Horvath, C.M., 2000. Interferon regulatory factor subcellular localization is determined by a bipartite nuclear localization signal in the DNA-binding domain an d interaction with cytoplasmic retention factors. Proc. Natl. Acad. Sci. 97, 7278–7283.
Li, J., Tian, Y., Liu, J., Wang, C., Feng, C., Wu, H., Feng, H., 2018. Lysine 39 of IKKε of black carp is crucial for its regulation on IRF7-mediated antiviral signaling. Fish Shellfish Immunol. 77, 410–418.
Li, J., Yan, C., Liu, J., Yan, J., Feng, H., 2019. SIKE of black carp is a substrate of TBK1 and suppresses TBK1-mediated antiviral signaling. Dev. Comp. Immunol. 90, 157–164.
Li, S., Lu, L.F., Feng, H., Wu, N., Chen, D.D., Zhang, Y.B., Gui, J.F., Nie, P., Zhang, Y.A., 2014. IFN regulatory factor 10 is a negative regulator of the IFN responses in fish. J. Immunol. 193 (3), 1100–1109.
Lim, C.P., Cao, X., 2006. Structure, function, and regulation of STAT proteins. Mol. Biosyst. 2 (11), 536–550.
Liu, J., Li, J., Xiao, J., Chen, H., Lu, L., Wang, X., Feng, H., 2017. The antiviral signaling mediated by black carp MDA5 is positively regulated by LGP2. Fish Shellfish Immunol. 66, 360–371.
Lu, L., Wang, X., Wu, S., Song, X., Zou, Z., Xie, X., Feng, H., 2017. Black carp STING functions importantly in innate immune defense against RNA virus. Fish Shellfish Immunol. 70, 13–24.
Meissl, K., Macho-Maschler, S., Müller, M., Strobl, B., 2017. The good and the bad faces of STAT1 in solid tumours. Cytokine 89, 12–20.
Najjar, I., Fagard, R., 2010. STAT1 and pathogens, not a friendly relationship. Biochimie 92 (5), 425–444.
Nan, J., Wang, Y., Yang, J., Stark, G.R., 2018. IRF9 and unphosphorylated STAT2 cooperate with NF-κB to drive IL6 expression. Proc. Natl. Acad. Sci. 115 (15), 3906–3911.
Palosaari, H., Parisien, J.P., Rodriguez, J.J., Ulane, C.M., Horvath, C.M., 2003. STAT protein interference and suppression of cytokine signal transduction by measles virus V protein. J. Virol. 77 (13), 7635–7644.
Paul, A., Tang, T.H., Ng, S.K., 2018. Interferon regulatory factor 9 structure and regulation. Front. Immunol. 9.
Paun, A., Pitha, P.M., 2007. The IRF family, revisited. Biochimie 89 (6–7), 744–753.
Pervolaraki, K., Talemi, S.R., Albrecht, D., Bormann, F., Bamford, C., Mendoza, J.L., Boulant, S., 2018. Differential induction of interferon stimulated genes between type I and type III interferons is independent of interferon receptor abundance. PLoS Pathog. 14 (11), e1007420.
Ruan, B.Y., Chen, S.N., Hou, J., Huang, B., Laghari, Z.A., Li, L., Nie, P., 2017. Two type II IFN members, IFN-γ and IFN-γ related (rel), regulate differentially IRF1 and IRF11 in zebrafish. Fish Shellfish Immunol. 65, 103–110.
Shi, J., Zhang, Y.B., Liu, T.K., Sun, F., Gui, J.F., 2012. Subcellular localization and functional characterization of a fish IRF9 from crucian carp Carassius auratus. Fish Shellfish Immunol. 33 (2), 258–266.
Shi, Y., Zhang, Y.B., Zhao, Z., Jiang, J., Zhang, Q.Y., Gui, J.F., 2008. Molecular characterization and subcellular localization of Carassius auratus interferon regulatory factor-1. Dev. Comp. Immunol. 32 (2), 134–146.
Sobhkhez, M., Skjesol, A., Thomassen, E., Tollersrud, L.G., Iliev, D.B., Sun, B., Jørgensen, J.B., 2014. Structural and functional characterization of salmon STAT1, STAT2 and IRF9 homologs sheds light on interferon signaling in teleosts. FEBS J. 4, 858–871.
Song, H., Yan, Y.L., Titus, T., He, X., Postlethwait, J.H., 2011. The role of Stat1b in zebrafish hematopoiesis. Mech. Dev. 128 (7–10), 442–456.
Song, X., Li, W., Xie, X., Zou, Z., Wei, J., Wu, H., Feng, H., 2019. NLRX1 of black carp suppresses MAVS-mediated antiviral signaling through its NACHT domain. Dev. Comp. Immunol. 96, 68–77.
Suprunenko, T., Hofer, M.J., 2016. The emerging role of interferon regulatory factor 9 in the antiviral host response and beyond. Cytokine Growth Factor Rev. 29, 35–43.
Tang, X., Gao, J.S., Guan, Y.J., McLane, K.E., Yuan, Z.L., Ramratnam, B., Chin, Y.E., 2007. Acetylation-dependent signal transduction for type I interferon receptor. Cell 131 (1), 93–105.
Tsuno, T., Mejido, J., Zhao, T., Morrow, A., Zoon, K.C., 2009. IRF9 is a key factor for eliciting the antiproliferative activity of IFN-α. J. Immunother. 32 (8), 803.
Wu, H., Zhang, Y.Y., Lu, X.Y., Xiao, J., Feng, P.H., Feng, H., 2019. STAT1a and STAT1b of black carp play important roles in the innate immune defense against GCRV. Fish Shellfish Immunol. 386–394.
Wu, Z., Wang, L., Xu, X., Lin, G., Mao, H., Ran, X., Xu, Q., 2017. Interaction of IRF9 and STAT2 synergistically up-regulates IFN and PKR transcription in Ctenopharyngodon idella. Mol. Immunol. 85, 273–282.
Xiao, J., Yan, C., Zhou, W., Li, J., Wu, H., Chen, T., Feng, H., 2017. CARD and TM of MAVS of black carp play the key role in its self-association and antiviral ability. Fish Shellfish Immunol. 63, 261–269.
Xu, M., Liu, P.P., Li, H., 2019. Innate immune signaling and its role in metabolic and cardiovascular diseases. Physiol. Rev. 99 (1), 893–948.
Yanai, H., Negishi, H., Taniguchi, T., 2012. The IRF family of transcription factors: inception, impact and implications in oncogenesis. OncoImmunology 1 (8), 1376–1386.
Yang, C., Liu, L., Liu, J., Ye, Z., Wu, H., Feng, P., Feng, H., 2019. Black carp IRF5 interacts with TBK1 to trigger cell death following viral infection. Dev. Comp. Immunol. 100, 103426.
Yang, Q., Cui, J., Song, W., Zhao, X., Xu, T., 2017. The evolution and functional characterization of miiuy croaker interferon regulatory factor 9 involved in immune response. Fish Shellfish Immunol. 66, 524–530.
Yuan, H., You, J., You, H., Zheng, C., 2018. Herpes simplex virus 1 UL36USP antagonizes type I Interferon-Mediated antiviral innate immunity. J. Virol. 92 (19) e01161-18.
Zhang, Y., Chen, Y., Yun, H., Liu, Z., Su, M., Lai, R., 2017. STAT1β enhances STAT1 function by protecting STAT1α from degradation in esophageal squamous cell carcinoma. Cell Death Dis. 8 (10), e3077.
Zhou, W., Zhou, J., Lv, Y., Qu, Y., Chi, M., Li, J., Feng, H., 2015. Identification and characterization of MAVS from black carp Mylopharyngodon piceus. Fish Shellfish Immunol. 43 (2), 460–468.